

Finite Element Analysis of Thermal Stresses in Functionally Gradient Layered Composites

Jin-Rae Cho* and Byung-Guk Kim**

(Received March 23, 1998)

A new composite material has been introduced which has a great potential satisfying successfully the desired functions under severe thermal circumstances. Because of the sharp material discontinuity at the interfaces between different material layers in classical layered composites, thermal and mechanical stress concentration may exist at such interfaces, and which results in undesired failure. The functionally gradient material (FGM), a new concept for future-oriented composite material, has a continuously varying material variation through the thickness of layered composites. And, hence, it can eliminate the defect occurred in classical layered composites. The purpose of this study is to develop a technique for finite element analysis of the thermal characteristics of FGMs, and to investigate the effects of significant governing parameters, a variation function of material composition and a relative thickness of FGM layer inserted between metal and ceramic layers. Through numerous numerical simulations carried out with the developed FEM program, we investigated the thermal characteristics for different concerning parameters. Considerable improvement and parametric dependence on temperature and thermal stress distributions are obtained.

Key Words: Functionally Gradient Material, Thermal Stress, Finite Element Analysis, Volume Fraction, Relative Thickness Ratio.

1. Introduction

Classical layered composite materials, thanks to a combination of superior properties of different materials such as metals and ceramics, have been widely used for various engineering applications. That is, to meet mutually different functions, they are made by composing of metals having high strength against fracture and thermal shock, and ceramic having low density, superior thermal strength and resistance against creep.

However, in classical layered composite, there may exist sort of stress concentration at the interface where two different material layers meet, which can produce undesired results such as excessive thermal stresses, occurrence of crack and

layer delamination. This defect is totally owing to the sharp discontinuity in material composition at such interfaces.

To overcome such a defect in classical layered composites, studies on the development of new layered composites, functionally gradient materials, have been intensively progressed since late 1980's. As illustrated in Fig. 1, FGM has a material composition varying continuously (without any discontinuity) through the thickness.

Among major merits of FGMs are ; (1) smooth variation in thermal stress distribution, (2) minimization of stress concentration occurred near interfaces or free edges and (3) controllability of design parameters.

The purpose of this study is to develop a numerical technique for finite element analysis and to carry out numerical simulations for its thermal stress characteristics. This paper is organized as follows ; (1) theoretical study of FGMs, (2) finite element approximation, (3) numerical

* Assistant Professor, School of Mechanical Engineering, Pusan National University, Jangeong-Dong, Kumjung-Ku, Pusan 609-735, Korea

** Graduate Research Assistant

results and (4) conclusion.

2. Variation of Material Composition

Referring to Fig. 3 of FGMs of uniform thickness $2c$, metal and ceramic compositions vary with their volume fraction changes through the thickness. If we denote volume fraction ratios of metal and ceramic, respectively, by f_m and f_c , then $f_m + f_c = 1$. So, it is enough for constructing a specific material composition to define a volume fraction function for any one material. Here, let us

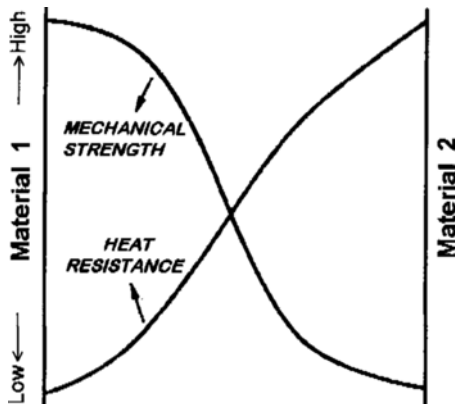
choose it of metal (i. e., f_m) such that (N is a real number)

$$f_m(y) = \begin{cases} 1, & (-c \leq y \leq -y_m) \\ \left[\frac{y_c - y}{y_c + y_m} \right]^N, & (-y_m \leq y \leq y_c) \\ 0, & (y_c \leq y \leq c) \end{cases} \quad (1)$$

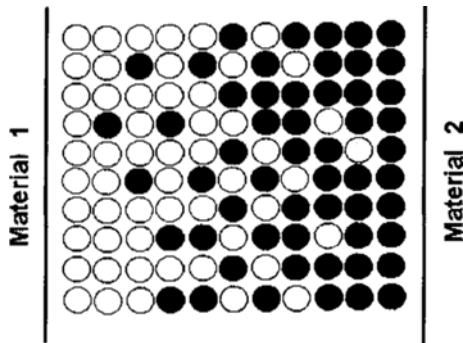
Here, y_m, y_c represent the vertical locations of bottom and top surface of the middle FGM layer. By a power index N is physically meant a parameter controlling the material composition variations through the thickness. Various patterns of volume fractions can be obtained for different values of N , which is well shown in Fig. 2.

Another important parameter is the relative thickness ratio RT of the middle FGM layer to the entire thickness $2c$, that is $RT = (y_c - y_m) / 2c$. According to the relative thickness ratio, we have the following major categories for FGM composites.

Next, we record the effective material properties of the middle FGM layer expressed by those of ceramic and metal and volume fraction functions, which are derived according to the modified



(a) Variation of thermomechanical properties



(b) Material composition

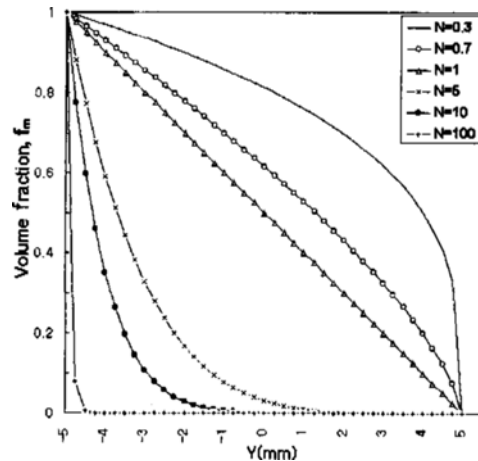


Fig. 2 Variations of the metal volume fraction.

Fig. 1 A functionally gradient material.

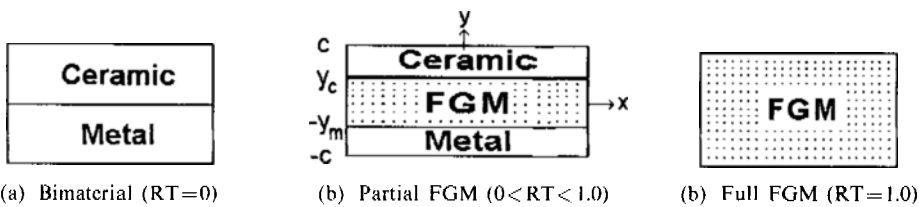


Fig. 3 Type of FGM layered composites.

Eshelby's equivalent inclusion method. More detailed derivation may referred to Wakashima and Tsukamoto(1991). Let us denote the bulk modulus by K , the shear modulus by μ , Young's modulus by E , Poisson's ratio by ν , the thermal expansion coefficient by α , the thermal conductivity by k and the specific heat by c .

The effective bulk modulus \bar{K} and shear modulus $\bar{\mu}$ are computed by the following relations.

$$\bar{K} = \frac{af_c K_m}{f_m K_c + af_c K_m} (K_c - K_m) + K_m \quad (2)$$

$$\bar{\mu} = \frac{bf_c \mu_m}{f_m \mu_c + bf_c \mu_m} (\mu_c - \mu_m) + \mu_m \quad (3)$$

Here, subscripts c and m indicate ceramic and metal, respectively, and

$$a = \frac{K_c (3K_m + 4\mu_m)}{K_m (3K_c + 4\mu_m)} \quad (4)$$

$$b = \frac{\mu_c (\mu_m + \mu_m e)}{\mu_m (\mu_c + \mu_m e)} = \frac{(1+e)\mu_c}{(\mu_c + e\mu_m)} \quad (5)$$

where, $e = (9K_m + 8\mu_m) / (6K_m + 12\mu_m)$. With \bar{K} , $\bar{\mu}$, effective Young's modulus \bar{E} , Poisson's ratio $\bar{\nu}$ and thermal expansion coefficient $\bar{\alpha}$ are expressed as follows from basic parametric relations and the Levin's relation

$$\bar{E} = \frac{9\bar{K}\bar{\mu}}{3\bar{K} + \bar{\mu}} \quad (6)$$

$$\bar{\nu} = \frac{3\bar{K} - 2\bar{\mu}}{2(3\bar{K} + \bar{\mu})} \quad (7)$$

$$\bar{\alpha} = \frac{K_c K_m (K_m - \bar{K})}{K K_m (K_m - K_c)} (\alpha_c - \alpha_m) + \alpha_m \quad (8)$$

Finally, the effective thermal conductivity \bar{k} and specific heat \bar{c} are

$$\bar{k} = \frac{f_c k_m (k_c - k_m)}{k_m + f_m (k_c - k_m)/3} + k_m \quad (9)$$

$$\bar{c} = c_c + (c_m - c_c) f_m \quad (10)$$

As for the effective density $\bar{\rho}$ which is directly proportional to the composition fraction, we immediately compute by the relation, $\bar{\rho}(y) = \rho_c + (\rho_m - \rho_c) f_m$.

3. Analysis Model and Heating Condition

For our numerical study, we select Ni for metal layer and aluminum oxide(hereafter, Al_2O_3) for

ceramic layer. The main reasons for selecting these materials are : (1) they are widely used, (2) their material properties are suitable for composites and (3) their material data are well known. In Table 1, we contain material data of Ni and Al_2O_3 .

A geometry of symmetric FGM model (a transversely isotropic material) for finite element analysis is shown in Fig. 4, where $2L=20\text{mm}$ and $2c=10\text{mm}$. Since we made the assumption of infinite dimension in the x-axis, we apply the symmetric boundary condition (i. e., $\partial T / \partial x = 0$ on the sides of $x = \pm L$). In order to construct finite element mesh, we use isoparametric bilinear two dimensional quadrilateral elements.

Referring to Fig. 4, we made the following assumptions and conditions for this study.

- (1) Neglecting creeps in Ni and Al_2O_3 .
- (2) Perfect bonding.
- (3) Initially stress-free state.
- (4) Temperature independent material constants.

And the model types of FGM consist of ; (1) classical bimaterial, (2) partial FGM and (3) full FGM, as shown in Fig. 3.

Table 1 Thermal and mechanical properties.

Material	Ni	Al_2O_3
Density (kg/m^3)	8900.0	3970.0
Specific heat ($\text{J}/\text{Kg} \cdot ^\circ\text{K}$)	444.0	775.0
Thermal conductivity ($\text{W}/\text{m} \cdot ^\circ\text{K}$)	90.7	30.1
Young's modulus (Gpa)	199.5	393.0
Poisson's ratio	0.3	0.25
Thermal expansion ($^\circ\text{K} \times 10^{-6}$)	13.3	8.8

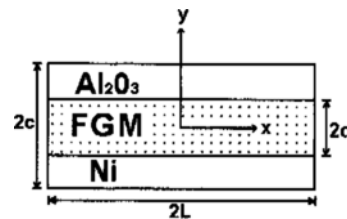


Fig. 4 A symmetric FGM model for finite element analysis.

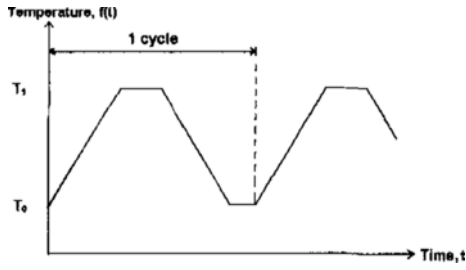


Fig. 5 Heating cycle.

As for thermal conditions, constant room temperature T_0 is applied to the bottom surface of a FGM, and thermal cycling shown in Fig. 5 is applied to the top surface, where T_0 is 290 K and T_1 is 1290 K. A heating cycle consists of four steps ; a heating during 40 s, a upkeeping(5 s), a cooling(40 s) and a upkeeping(5 s).

4. Formulation for Numerical Approximation

For our numerical approximations, let us consider a two dimensional semi-infinite(in the x-axis) FGM (i. e., $\Omega = (-\infty, \infty) \times (-c, c)$) with a smooth boundary $\partial\Omega$). Then, the governing equations are composed of a heat diffusion equation and initial and boundary conditions(i. e., initial-boundary-value problem):

$$\left. \begin{aligned} \nabla \cdot (k \nabla T) + \frac{\partial q}{\partial t} &= \rho c \frac{\partial T}{\partial t}, \text{ in } (0, t^*] \times \Omega \\ T &= T_0, \text{ at } t=0 \\ T &= T_0, \text{ on } y=-c \\ T &= f(t), \text{ on } y=c \end{aligned} \right\} \quad (11)$$

where, ∇ is a two-dimensional gradient operator and $f(t)$ is a cyclic function, as shown in Fig. 5, and t^* denotes a considering time interval.

To formulate numerical approximations for the above partial differential equation, we need to discretize it in time domain and to take a variational formulation in space coordinates.

First, for a time-discretization, let us make a uniform time partition such that $t^* = N\Delta t$ and $t^{n+1} = t^n + \Delta t$ ($n=0, 1, \dots, N-1$). For our study, we use the well-known second order Crank-Nicolson method (Zienkiewicz and

Taylor, 1991), for which T and $\frac{\partial T}{\partial t}$ at time-step $t^{n+1/2}$ are approximated with T^n and T^{n+1} ,

$$T^{n+1/2} \approx \frac{1}{2} (T^{n+1} + T^n) \quad (12)$$

$$\left(\frac{\partial T}{\partial t}\right)^{n+1/2} \approx \frac{1}{\Delta t} (T^{n+1} - T^n) \quad (13)$$

Assuming no q and plugging Eqs. (12) and (13) into Eq. (11), we have the semi-discrete expression at time-step t^{n+1} given by

$$\rho c \left(\frac{T^{n+1} - T^n}{\Delta t}\right) = \nabla \cdot k \nabla \left(\frac{T^{n+1} + T^n}{2}\right) \quad (14)$$

Next, for Galerkin variational formulation for T at time-step t^{n+1} , let us define the test space V (Ω) of admissible temperature functions $Q(x, y)$ and the trial function space $\tilde{V}_n(\Omega)$ such as

$$\left. \begin{aligned} V(\Omega) &= \{Q: Q \in H^1(\Omega) | Q=0 \text{ on } y=\pm c\} \\ \tilde{V}_n(\Omega) &= V(\Omega) + \{f^*\}_n \end{aligned} \right\} \quad (15)$$

Here, $H^1(\Omega)$ is a Hilbert space(Adams, 1978) and $\{f^*\}_n$ are $H^1(\Omega)$ functions which have T_0 at $y=-c$ and $f(t^n)$ at $y=c$. Then, using divergence theorem with an arbitrary test function $Q \in V(\Omega)$, we obtain the following.

$$\int_{\Omega} \left\{ \rho c \left(\frac{T^{n+1} - T^n}{\Delta t}\right) Q + k \nabla \left(\frac{T^{n+1} + T^n}{2}\right) \cdot \nabla Q \right\} d\Omega = \int_{\partial\Omega} Q \left\{ k \nabla \left(\frac{T^{n+1} + T^n}{2}\right) \cdot n \right\} ds \quad (16)$$

From our previous assumptions and boundary conditions, the RHS vanishes and finally the variational formulation arrives at the Crank-Nicolson-Galerkin scheme:

Given T^0 , find $T^{n+1} \in \tilde{V}_{n+1}(\Omega)$ such that ($n=0, 1, \dots, N-1$)

$$\int_{\Omega} \rho c T^{n+1} Q d\Omega - \int_{\Omega} \rho c T^n Q d\Omega = -\frac{\Delta t}{2} \int_{\Omega} \left\{ k \nabla (T^{n+1} + T^n) \cdot \nabla Q \right\} d\Omega, \forall Q \in V(\Omega) \quad (17)$$

It is widely known that this scheme is unconditionally convergent for any choice of time partitioning Δt and the finite element mesh size (but with oscillation problem).

For finite element approximations, we express trial function T_h^{n+1} and test function Q_h using bilinear finite element basis functions $\{\psi_j\}_{j=1}^M$; $\text{span} \{\psi_j\}_{j=1}^M = V^h(\Omega)$ (finite element approxima-

tion space) by

$$\left. \begin{aligned} T_h^{n+1} &= \sum_{j=1}^M T_{h,j}^{n+1} \phi_j(x, y) \\ Q_h &= \sum_{i=1}^M \beta_i \psi_i(x, y) \end{aligned} \right\} \quad (18)$$

Substituting the expansions in Eq. (18) into Eq. (17) and employing a matrix form, we obtain the full-discrete approximation,

$$\begin{aligned} &\text{Given } T_h^0, \text{ find } T_h^{n+1} \in \tilde{V}^h(\Omega) \text{ such that} \\ &(\mathbf{n}=0, 1, \dots, \mathbf{N}-1) \\ &\left\{ [C] + \frac{\Delta t}{2} [K] \right\} \{ T_h^{n+1} \} = \left\{ [C] - \frac{\Delta t}{2} [K] \right\} \\ &\{ T_h^n \} \quad \forall Q_h \in V^h(\Omega) \end{aligned} \quad (19)$$

where,

$$\left. \begin{aligned} C_{ij} &= \int_{\Omega} \rho c \phi_i \phi_j d\Omega \\ K_{ij} &= \int_{\Omega} \left(k \frac{\partial \phi_i}{\partial x} \frac{\partial \phi_j}{\partial x} + k \frac{\partial \phi_i}{\partial y} \frac{\partial \phi_j}{\partial y} \right) d\Omega \end{aligned} \right\} \quad (20)$$

After we construct two matrices $[C]$ and $[K]$, we obtain approximate temperature distribution $T(x, y; t)$ successively through a system of simultaneous Eq. (19).

Once computing temperature distribution, thermal stress distributions at any time are calculated. According to the elementary engineering relations based on the assumptions of infinitesimal strains and plane stress condition, a non-vanishing strain (i. e., ε_{xx}) is

$$\varepsilon_{xx}(y) = \varepsilon(y) = \varepsilon_0 + \kappa_0 y \quad (21)$$

where, ε_0 and κ_0 represent, respectively, the strain and the curvature of the mid-surface (i. e. $y=0$). Therefore, a non-vanishing thermal stress (i. e., σ_{xx}) at time-step t^n is expressed by

$$\begin{aligned} \sigma_{xx}^n(y) &= \sigma^n(y) = E(y) [\varepsilon(y) - \alpha(y) \Delta T^n(y)] \\ &= E(y) [\varepsilon_0 + \kappa_0 y - \alpha(y) \Delta T^n(y)] \end{aligned} \quad (22)$$

with $\Delta T^n(y)$ being denoted by $(T^n(y) - T_0)$ at arbitrary time-step t^n .

Since the resultant force and moment produced by thermal stress should be statically equilibrated with applied external force F^{ap} and applied external moment M^{ap} , ε_0 and κ_0 in Eq. (22) can be determined by the following relations:

$$\varepsilon_0 = \frac{-I_2(J_0 + F^{ap}) + I_1(J_1 + M^{ap})}{I_1^2 - I_0 I_2} \quad (23)$$

$$\kappa_0 = \frac{I_1(J_0 + F^{ap}) - I_0(J_1 + M^{ap})}{I_1^2 - I_0 I_2} \quad (24)$$

Here,

$$I_i = \int_{-c}^c y^i E(y) dy \quad (25)$$

$$J_i = \int_{-c}^c y^i E(y) \alpha(y) \Delta T^n(y) dy \quad (26)$$

Inserting ε_0 and κ_0 into Eq. (22) with no application of external force and moment, we finally obtain the equation for thermal stress distribution through the thickness at time-step t^n

$$\begin{aligned} \sigma^n(y) &= E(y) \left[\frac{-I_2 J_0 + I_1 J_1 + (I_1 J_0 - I_0 J_1) y}{I_1^2 - I_0 I_2} \right. \\ &\quad \left. - \alpha(y) \Delta T^n(y) \right] \end{aligned} \quad (27)$$

5. Numerical Experiments

We carried out numerical experiments to investigate thermal stress characteristics of the FGM composed of Ni and Al_2O_3 with the finite element technique developed according to the previous analytic results and approximation formulations. To observe the effects of the two considering parameters, RT and N, we tested the cases of $N=0.3, 0.7, 1, 5, 10,$ and 100 for each RT of $0.2, 0.5, 0.7$ and 1 . For a clear comparison between classical and FGM layered composites, we include the bimaterial case in each figure.

In Figs. 6–9, temperature distributions, when the top surface is heated to 1290 K, are presented. For the bimaterial (RT=0), a remarkable temperature gradient exists at the interface of two material layers. Also, big temperature gradients prevail as N increases or approaches 0, particularly for the smaller RT. But, temperature distributions for every N become smoother as RT increases. This tendency is due solely to an extension of the middle FGM layer.

Next four figures, Figs. 10–13 show thermal stress distributions through the thickness when the top surface is heated to T_1 . Here, we pay particular attention to the variation in thermal stresses at the interfaces for different relative thicknesses and the material compositions.

From Fig. 10 of RT=0.2, stress concentration for $N=0.3$ at the interface between FGM and

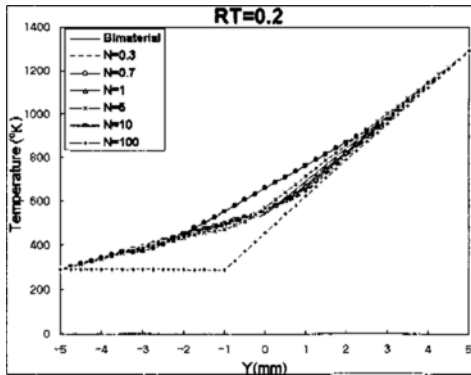


Fig. 6 Temperature distribution (RT=0.2).

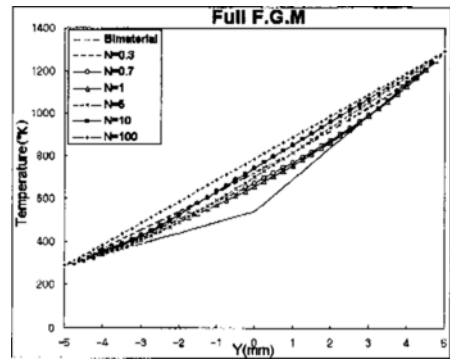


Fig. 9 Temperature distribution (Full FGM).

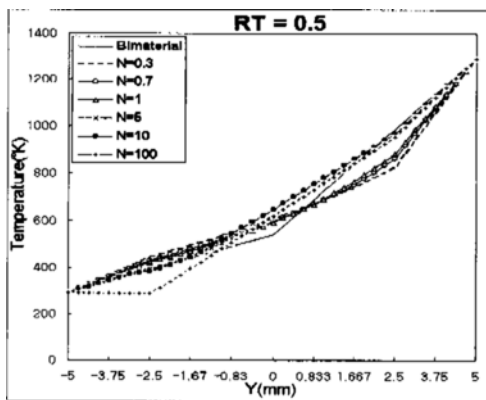


Fig. 7 Temperature distribution (RT=0.5).

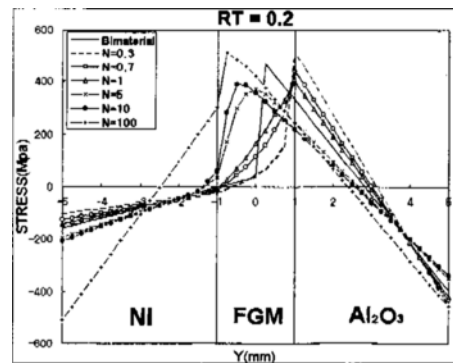


Fig. 10 Thermal stress distribution (RT=0.2).

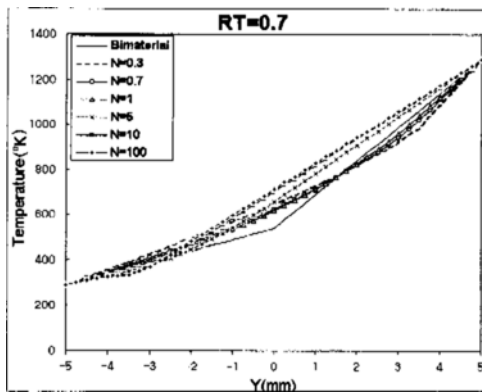


Fig. 8 Temperature distribution (RT=0.7).

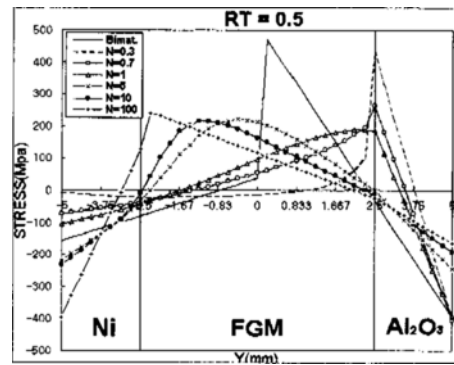


Fig. 11 Thermal stress distribution (RT=0.5).

ceramic layers becomes to be relaxed by increasing N , however when N exceeds a certain value, the other interface has stress concentration, too. The reason of the stress concentration occurred for lower or higher values of N is because the middle FGM layer approaches, respectively,

metal or ceramic layer, i.e., a classical nonsymmetric bimaterial composite (referring to Fig. 3).

From Fig. 11 to Fig. 13, it is observed that maximum thermal stresses decrease as RT increases for $N > 0.3$. For the case of $N = 0.3$, a steep increase in thermal stress distribution at the right interface can not be weakened even as RT increases. This can also be explained by the fact

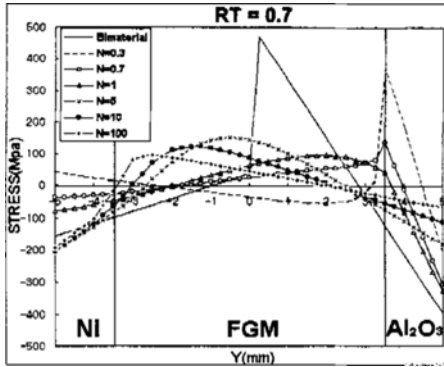


Fig. 12 Thermal stress distribution (RT=0.7).

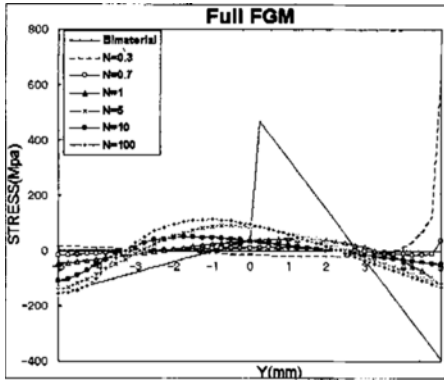


Fig. 13 Thermal stress distribution (Full FGM).

explained just above. In particular, for the full FGM ($N > 0.3$), smoother thermal stress distributions having smaller values are obtained.

In next figures, Fig. 14 and Fig. 15, we plotted the estimated global and local sharpnesses, S_G and S_L , respectively. These two quantities measure the sharpness of variations in thermal stresses in the middle FGM layer. The first quantity S_G is defined as

$$S_G = \frac{|\sigma_{\max} - \sigma_{\min}|}{RT} \quad (28)$$

and the second quantity S_L is defined as the inverse of two times of the shorter distance between the locations $y_0, y_{1/\sqrt{2}}$ at which thermal stress reaches the steepest value σ_0 and it drops by Δ_N , respectively (Here, Δ_N means the relative difference σ_0 and $\sigma_0/\sqrt{2}$ for each N when $RT=0.2$).

$$S_L = \frac{1}{2|y_0 - y_{1/\sqrt{2}}|} \quad (29)$$

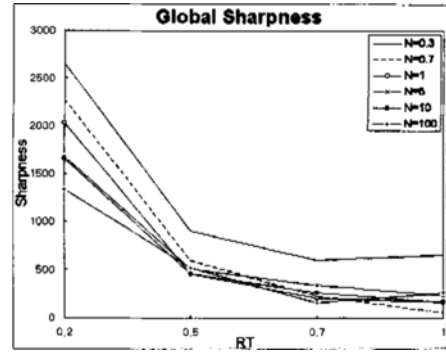


Fig. 14 Estimated global sharpness, S_G .

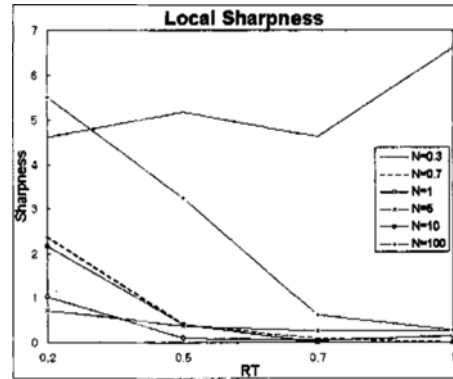


Fig. 15 Estimated local sharpness, S_L .

From Fig. 14, the estimated global sharpnesses strictly decrease as RT approaches unity except for $N=0.3$ and 100. While, from Fig. 15, the estimated local sharpnesses decrease as RT approaches unity except for $N=0.3$.

From the numerical results obtained in this study, we can observe that, with appropriate choice of these two parameters, we can eliminate steep increase in thermal stress at the interfaces and can produce smaller and smoother thermal stress distributions. However, it is worth to note that, with reasonably low N or small RT with reasonably low or high values of N , we can not improve thermal characteristics, because these two limiting cases correspond to classical bimaterial composites, as shown in Fig. 3(a).

6. Conclusion

In this paper, we addressed a technique for finite element analysis and parametric investiga-

tion of thermal characteristics of FGMs, and presented numerical results illustrating the effects of two parameters.

From numerical results, we confirm that considerable improvement is possible by inserting FGM layer between metal and ceramic layers in classical bimaterial layered composites. Also, according to variations of two major parameters, different thermal stress characteristics were observed for different choices of parameters. In our model problem, temperature and stress distribution become smoother when RT approaches unity and for a selective range of N .

Therefore, the optimal FGM that can satisfy the desired thermomechanical functions with minimum stress concentration at the layer interfaces would be expected by controlling two governing parameters, and which deserves the future work.

Acknowledgments

The financial support for this work by Pusan National University under Grant-in-Scientific-Assistance (1997, 10-1998, 9) is gratefully acknowledged.

References

Mortensen, A. and Suresh, S., 1995, "Functionally Graded Metals and Metal-Ceramic Composites : Part 1, Processing," *International Materials Review*, Vol. 40, No. 6, pp. 239~265.

Holt, J. B., Koizumi, M., Hirai, T. and Munir, Z. A., 1993, "Ceramic Transactions ;Functionally Gradient Materials," Vol. 34, *The American Ceramic Society*.

Giannakopoulos, A. E., Suresh, S., Finot, M. L. and Olsson, M., 1995, "Elastoplastic Analysis of Thermal Cycling : Layered Material with Compositional Gradient," *Acta Metall. Mater.*,

Vol. 43, No. 4, pp. 1335~1354.

Suresh, S., Giannakopoulos, E. and Olsson, M., 1994, "Elastoplastic Analysis of thermal Cycling : Layered Materials with Sharp Interfaces," *J. Mech. Phys. Solids.*, Vol. 42, No. 6, pp. 979~1018.

Williamson, R. L., Rabin, B. H. and Drake, J. T., 1993, "Finite Element Analysis of Thermal Residual Stresses at Graded Ceramic Metal Interfaces. Part 1. Model Description and Geometrical Effects," *J. Appl. Phys.*, Vol. 74, No. 2, pp. 1310~1320.

Wakashima, K. and Tsukamoto, H., 1991, "Mean-Field Micromechanics Model and Its Application to the Analysis of Thermomechanical Behaviour of Composite Materials," *Materials Science and Engineering*, Vol. A146, pp. 291~316.

Morjaria, M. and Mukherjee, S., 1981, "Finite Element Analysis of Time-Dependent Inelastic Deformation in the Presence of Transient Thermal Stresses," *J. for Numerical Methods in Engineering*, Vol. 17, pp. 909~921

Freund, L. B., 1993, "The Stress Distribution and Curvature of a General Compositionally Graded Semiconductor Layer," *J. Crystal Growth*, Vol. 132, pp. 341~344.

Ravichandran, K. S., 1994, "Elastic Properties of Two-Phase Composites," *J. Am. Ceram. Soc.*, Vol. 77, No. 5, pp. 1178~1184.

Nakajima, K., 1992, "Calculation of Stress in GaAs/Si Strained Heterostructures," *J. Crystal Growth*, Vol. 121, pp. 278~296.

Timoshenko, S. P. and Goodier, J. N., 1970, *Theory of Elasticity*, McGraw-Hill.

Zienkiewicz, O. C. and Taylor, R. L., 1991, *The Finite Element Method*, Vol. 2, McGraw-Hill.

Adams, R. A., 1978, *Sobolev Spaces*, Academic Press.